



DIGITAL ACCESS TO SCHOLARSHIP AT HARVARD

How the Motility Pattern of Bacteria Affects Their Dispersal and Chemotaxis

The Harvard community has made this article openly available.
[Please share](#) how this access benefits you. Your story matters.

Citation	Taktikos, Johannes, Holger Stark, and Vasily Zaburdaev. 2013. "How the Motility Pattern of Bacteria Affects Their Dispersal and Chemotaxis." PLoS ONE 8 (12): e81936. doi:10.1371/journal.pone.0081936. http://dx.doi.org/10.1371/journal.pone.0081936 .
Published Version	doi:10.1371/journal.pone.0081936
Accessed	February 19, 2015 3:11:46 PM EST
Citable Link	http://nrs.harvard.edu/urn-3:HUL.InstRepos:11879562
Terms of Use	This article was downloaded from Harvard University's DASH repository, and is made available under the terms and conditions applicable to Other Posted Material, as set forth at http://nrs.harvard.edu/urn-3:HUL.InstRepos:dash.current.terms-of-use#LAA

(Article begins on next page)

How the Motility Pattern of Bacteria Affects Their Dispersal and Chemotaxis

Johannes Taktikos^{1,2,3*}, Holger Stark², Vasily Zaburdaev^{1,3}

1 Max-Planck-Institut für Physik komplexer Systeme, Dresden, Germany, **2** Technische Universität Berlin, Institut für Theoretische Physik, Berlin, Germany, **3** Harvard University, School of Engineering and Applied Sciences, Cambridge, Massachusetts, United States

Abstract

Most bacteria at certain stages of their life cycle are able to move actively; they can swim in a liquid or crawl on various surfaces. A typical path of the moving cell often resembles the trajectory of a random walk. However, bacteria are capable of modifying their apparently random motion in response to changing environmental conditions. As a result, bacteria can migrate towards the source of nutrients or away from harmful chemicals. Surprisingly, many bacterial species that were studied have several distinct motility patterns, which can be theoretically modeled by a unifying random walk approach. We use this approach to quantify the process of cell dispersal in a homogeneous environment and show how the bacterial drift velocity towards the source of attracting chemicals is affected by the motility pattern of the bacteria. Our results open up the possibility of accessing additional information about the intrinsic response of the cells using macroscopic observations of bacteria moving in inhomogeneous environments.

Citation: Taktikos J, Stark H, Zaburdaev V (2013) How the Motility Pattern of Bacteria Affects Their Dispersal and Chemotaxis. PLoS ONE 8(12): e81936. doi:10.1371/journal.pone.0081936

Editor: James P. Brody, University of California Irvine, United States of America

Received: September 4, 2013; **Accepted:** October 25, 2013; **Published:** December 31, 2013

Copyright: © 2013 Taktikos et al. This is an open-access article distributed under the terms of the Creative Commons Attribution License, which permits unrestricted use, distribution, and reproduction in any medium, provided the original author and source are credited.

Funding: The authors acknowledge financial support by the Deutsche Forschungsgemeinschaft (DFG) through the Research Training Group GRK 1558 "Nonequilibrium Collective Dynamics in Condensed Matter and Biological Systems". The funders had no role in study design, data collection and analysis, decision to publish, or preparation of the manuscript.

Competing Interests: The authors have declared that no competing interests exist.

* E-mail: taktikos@pks.mpg.de

Introduction

Bacteria constitute a major part of the biomass on our planet [1]. They come in different shapes and sizes and are able to swim in water and crawl on surfaces [2]. Bacteria build complex colonies called biofilms [3] and find ways to adapt to the harshest environmental conditions [4]. One of the ways cells react to changes in the environment is by employing various "taxis-strategies". In response to gradients in temperature, chemicals, or electric fields [5], bacteria are able to alternate their motility to locate favorable niches and avoid dangerous locations. Chemotaxis is one of the best studied examples of this behavior and its biochemical mechanisms in bacteria are rather well understood [6]. However, bacteria moving in homogeneous environments often have a very distinct motility pattern, which is defined by the phenotype of the cell. It remains unclear how different motility patterns of bacteria can affect their ability to perform chemotaxis. In this paper, we propose a generalized random walk description of a broad class of observed bacterial motility patterns. It allows us to describe quantitatively the dispersal process of bacteria and calculate the effect of the motility pattern on the chemotactic behavior of the cells. This rigorous description creates the possibility of accessing additional information about the intrinsic response of the cells using macroscopic observations of bacteria moving in constant gradients or towards the point source of a chemical.

The run-and-tumble motion of *E. coli* bacteria is probably the best-known example of bacterial swimming. *E. coli* has multiple flagella, which can rotate and propel the cell forward. Flagella rotating in the counterclockwise (CCW) direction form a bundle

and the cell is in the "run" mode of highly persistent motion. When one or several flagella reverse the direction of rotation, the bundle comes apart and the cell body performs an irregular tumbling motion [7]. Usually, there is little displacement during the "tumbling" mode and it mainly serves to reorient the direction of the cell for the next run. For *E. coli*, the turning angles are randomly distributed with an average of about 70°. Many marine bacteria, such as *S. putrefaciens* or *P. haloplanktis* [8], that have just a single flagellum simply reverse the direction of their swimming when the flagellum switches the direction of rotation; this results in a turning angle distribution peaked around 180°. Interestingly, the run-reverse strategy is not exclusive to swimming cells but was also observed for bacteria moving on surfaces. Some bacteria, as for example *M. xanthus* [9,10], can also use different cell appendages called pili [11,12] or even more complex mechanisms, to attach to and actively move on surfaces. In this case, the alternation of pili activity on different poles of elongated cells also leads to the run-reverse motility pattern.

In response to changing environmental conditions, like a difference in concentration of a certain signaling chemical or nutrient, bacteria are able to regulate the durations of their run phases [13]. On average, runs become longer if a bacterium moves towards the source of the attracting signal and shortened if it moves away from the source [5,14]. It is important that in bacteria the probability to tumble or to continue a run depends on the concentration of the chemical sampled by the cell during its motion for a certain time interval, weighted by the internal response function of the cell [15]. Therefore, the chemotactic behavior and the motility pattern of bacteria are tightly coupled

together. Recently, another pattern of swimming was reported for *V. alginolyticus* bacteria [16]. These marine bacteria also have one flagellum, but during each second reversal its rotation is unstable and leads to a random turn of the cell body [17,18]. Hence, a trajectory of these bacteria is composed of strictly alternating 180° reversals and random turns with an average of 90°. Remarkably, *V. alginolyticus* were three times faster in gathering around the source of a chemoattractant when compared to *E. coli* [16,19]. To test if such an increased performance during chemotaxis can be attributed to their peculiar motility pattern, we developed a random walk model describing the trajectories of bacteria. It allowed us to calculate analytically the diffusion constants in the absence of the chemical and the drift speeds in a small linear gradient of chemoattractant. In particular, we show that the motility pattern alone cannot explain the experimentally observed difference between the chemotactic behavior of *V. alginolyticus* and *E. coli*. This strongly suggests that, instead, a difference in the response functions of the bacteria is the key feature that leads to the distinct behaviors observed experimentally. Our model can serve as an analytical tool to test for various response strategies of individual cells and relate them to the observed macroscopic agglomeration dynamics.

Motility patterns

We start with a brief description of three distinct motility patterns exhibited by bacteria. It appears that the motility of quite a large part of studied or practically relevant bacterial species can be attributed to one of these three classes. We first focus on a two-dimensional setup, since many tracking experiments for swimming cells are performed in planar geometry and surface-related motility is naturally two-dimensional. We will however show how to generalize our results to higher dimensions.

Swimming *E. coli* alternate persistent runs with tumbling events (see Fig. 1a). The duration of tumbles on average is about ten times shorter than the duration of runs, and in our model we will assume this time to be vanishingly small (however, see also Ref. [20], where tumbling times were explicitly modeled). The distribution of run times is well approximated by the exponential function with a mean value of ~1 s [13]. Recent experiments on tethered cells and accompanying theoretical analysis also suggest the possibility of run times with a power-law distribution [21,22]. Each run does not follow a perfectly straight line. The interaction of the cell body and flagella with the surrounding fluid results in a fluctuating direction of the cell velocity, which can be well described by rotational diffusion [13]. The speed of the cell during a single run and from one run to another is nearly constant [14,23]. Depending on the environmental conditions, the typical speed of *E. coli* is in the range of 15–30 μm s⁻¹ [13,24]. After a tumbling event, the new direction of swimming has on average an angle of 71° with the direction of the previous run [13].

Up to 70% of marine bacteria [25] and also bacteria twitching on surfaces, such as *P. aeruginosa* or *M. xanthus*, adopt a similar strategy to that of *E. coli*, but with 180° reorientation events (see Fig. 1b). The speed of their forward and backward motion is usually comparable [26]. Note that the run speeds of marine bacteria can reach up to 400 μm s⁻¹ [27], whereas cells twitching on a surface are much slower with typical speeds of ~0.1 μm s⁻¹ [28]. The motility pattern of another marine bacterium, *V. alginolyticus*, is similar to the run-reverse strategy. However, the flagellum of these cells is unstable when its rotation switches from CW to CCW direction, leading to the appearance of “flicks” – completely randomizing turning angles with an average of 90° (see Fig. 1c) [16]. Durations and speeds of runs after reversal or flick are fairly similar [16].

Analysis

To describe quantitatively the dynamics of dispersal of the bacteria exhibiting the above motility patterns, we propose the following generalized random walk model. Each random walker representing a single bacterium moves with velocity $\mathbf{v}(t) = v\mathbf{e}(t)$, where the speed $v = |\mathbf{v}(t)|$ is constant and the unit vector $\mathbf{e}(t) = (\cos \varphi(t), \sin \varphi(t))$ denotes the direction of propagation at time t , see Fig. 2. Integration of the velocity with respect to time yields the particle’s trajectory $\mathbf{r}(t) = \mathbf{r}(0) + \int_0^t dt' \mathbf{v}(t')$. It will be our first goal to determine the velocity autocorrelation function

$$C(t_1, t_2) = \langle \mathbf{v}(t_1) \cdot \mathbf{v}(t_2) \rangle, \tag{1}$$

where $\langle \dots \rangle$ denotes the ensemble average. It is directly connected to the mean squared displacement (MSD) via the Kubo relation

$$\langle [\mathbf{r}(t) - \mathbf{r}(0)]^2 \rangle = \int_0^t dt_1 \int_0^{t_1} dt_2 \langle \mathbf{v}(t_1) \cdot \mathbf{v}(t_2) \rangle. \tag{2}$$

If the MSD is a linear function of t for large times, the diffusion coefficient can be defined as $D = \lim_{t \rightarrow \infty} \langle [\mathbf{r}(t) - \mathbf{r}(0)]^2 \rangle / (2dt)$, where d is the spatial dimension [29,30]. Durations of runs are random and described by the probability density function (PDF) $f(\tau)$. For the model with two types of events we will allow for two separate PDFs of the run time after the corresponding reversal (r) or flick (f) event, $f_{r,f}(\tau)$. When a run is interrupted by a turning event (tumbling or reversal), the particle’s direction of motion changes instantaneously by an angle φ , drawn from the probability density

$$g(\varphi) = \frac{1}{2} [\delta(\varphi - \varphi_0) + \delta(\varphi + \varphi_0)], \tag{3}$$

where $\varphi_0 \sim 71^\circ$ for run-and-tumble of *E. coli* and $\varphi_0 \sim 180^\circ$ for run-reverse motion. Note that assuming a delta-peaked distribution for $g(\varphi)$ is a minor simplification; as we also show in Sec. III of Text S1, our results do not change if one considers a continuous distribution which leads to the same persistence parameter $\alpha = \langle \cos \varphi \rangle$. The turning angles for run-reverse and flick mode will be alternately chosen as $\pm 180^\circ$ (r) and $\pm 90^\circ$ (f).

In the case of constant speed, the correlation function $C(t_1, t_2)$ is determined by the dynamics of the angle $\varphi(t)$ describing the direction of the cell’s motion,

$$C(t_1, t_2) = v^2 \langle \cos[\varphi(t_2) - \varphi(t_1)] \rangle = v^2 \Re \langle e^{-i[\varphi(t_2) - \varphi(t_1)]} \rangle, \tag{4}$$

where \Re denotes the real part; note that, for symmetry reasons, the imaginary part vanishes after averaging. The random walk dynamics of the angle $\varphi(t)$ can be decomposed into two parts,

$$\varphi(t) = \varphi_{\text{rw}}(t) + \varphi_{\text{rot}}(t), \tag{5}$$

where $\varphi_{\text{rw}}(t)$ models the actual random walk due to a specific motility pattern with straight paths and jumps in the angle given by Eq. (3), and $\varphi_{\text{rot}}(t)$ describes angular changes due to rotational diffusion. It is natural to assume that the effects of fluctuations during the runs are independent of the reorientation events resulting from tumbles and reversals. Therefore, the averaging in Eq. (4) can be decoupled into

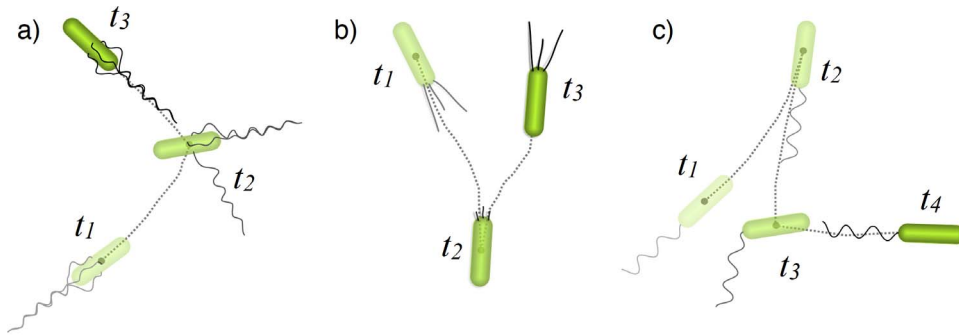


Figure 1. Sketch of the predominant motility patterns. a) Run-and-tumble, b) Run-reverse, and c) Run-reverse-flick. During a “run” event, a cell moves with high persistence. Runs are interrupted by reorientation events like tumbling or reversal. The time steps $t_1 < t_2 < t_3 < t_4$ indicate the sequence of these events. An average turning angle after tumbling in *E. coli* bacteria is $\sim 70^\circ$ (a), whereas it is an almost perfect reversal of 180° for many marine bacteria, or cells with twitching motility due to cell appendages, called pili (b). *V. alginolyticus* (c) alternates reversals (at t_2) with randomizing flicks (at t_3) with an average turning angle of 90° . doi:10.1371/journal.pone.0081936.g001

$$\langle e^{-i\Delta\varphi} \rangle = \langle e^{-i\Delta\varphi_{rw}} \rangle \langle e^{-i\Delta\varphi_{rot}} \rangle, \quad (6)$$

where $\Delta\varphi = \varphi(t_2) - \varphi(t_1)$. The velocity correlation function factorizes into a pattern-specific part $C_{rw}(t_1, t_2)$ and a factor due to rotational diffusion $C_{rot}(t_1, t_2)$:

$$C(t_1, t_2) = C_{rw}(t_1, t_2) \times C_{rot}(t_1, t_2). \quad (7)$$

The latter is known to be $C_{rot}(t_1, t_2) = \exp(-|t_2 - t_1|/\tau_{rot})$, where $\tau_{rot} = 1/(2D_r)$ is the characteristic rotational diffusion time showing how fast a particle is forgetting its direction of motion, and D_r is the rotational diffusion constant [31]. The averaging of the random walk part $\langle e^{-i\Delta\varphi_{rw}} \rangle$ from Eq. (6) can be expressed as

$$\begin{aligned} \langle e^{-i\Delta\varphi_{rw}} \rangle &= \langle e^{-i[\varphi_{rw}(t_2) - \varphi_{rw}(t_1)]} \rangle \\ &= \int_{-\infty}^{+\infty} d\varphi_1 \int_{-\infty}^{+\infty} d\Delta\varphi e^{-i\Delta\varphi} P(\varphi_1, t_1; \Delta\varphi, t_2). \end{aligned} \quad (8)$$

Here, $P(\varphi_1, t_1; \Delta\varphi, t_2)$ is the joint probability density to find a particle with direction φ_1 at time t_1 and direction $\varphi_1 + \Delta\varphi$ at time t_2 . We define the Fourier transform of a function $g(\varphi)$ as $\tilde{g}(k) = \int_{-\infty}^{+\infty} d\varphi e^{-ik\varphi} g(\varphi)$, and observe that Eq. (8) corresponds to a double Fourier transform of P with respect to φ_1 and $\Delta\varphi$, where the corresponding coordinates in Fourier space are set to $k_1 = 0$ and $k_2 = 1$, respectively:

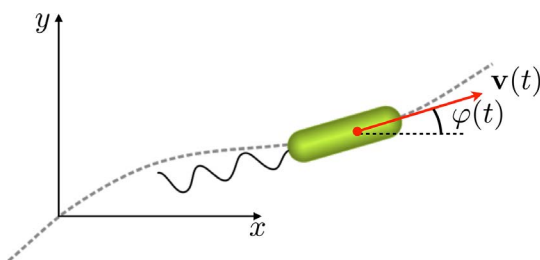


Figure 2. Setup of the model. A cell with velocity $\mathbf{v}(t)$ moves at constant speed v . The angle $\varphi(t)$ between the velocity vector $\mathbf{v}(t)$ and the x axis defines the direction of cell motion. doi:10.1371/journal.pone.0081936.g002

$$\langle e^{-i\Delta\varphi_{rw}} \rangle = \tilde{P}(k_1, t_1; k_2, t_2)|_{k_1=0, k_2=1}. \quad (9)$$

To find the joint PDF $P(\varphi_1, t_1; \Delta\varphi, t_2)$, we note that it is just a two-point density for a continuous time random walk model (CTRW) [32–34], where the angle φ performs this random walk. We now show how to solve the problem for the three motility patterns in question.

Results

Random walk with one turning angle

For run-and-tumble and run-reverse motion, the angular jump distribution $g(\varphi)$ is given by Eq. (3). In this case, we make use of a result from random walk theory for the joint probability P entering Eqs. (8, 9) [32–34] (see Sec. I of Text S1 for details). To proceed, we define the Laplace transform of a function $f(t)$ as $\hat{f}(s) = \mathcal{L}[f(t)](s) = \int_0^\infty dt e^{-st} f(t)$; the combined Fourier-Laplace transform of a function $h(\varphi, t)$ is denoted as $(k, s) = \int_0^\infty dt e^{-st} \int_{-\infty}^{+\infty} d\varphi e^{-ik\varphi} h(\varphi, t)$, where the Laplace transform corresponds to the variables $t \leftrightarrow s$ and the Fourier transform corresponds to $\varphi \leftrightarrow k$. After introducing the survival probability $F(\tau) = 1 - \int_0^\tau dt f(t)$, one obtains

$$\begin{aligned} \tilde{P}(k_1 = 0, p; k_2 = 1, s) = \\ \frac{\hat{F}(p)\hat{F}(s) + (\mathcal{L}[f(t_1 + \Delta t)](p, s) - \hat{F}(p)\hat{F}(s))(1 - \cos \varphi_0)}{[1 - \hat{f}(p)][1 - \hat{f}(s) \cos \varphi_0]}, \end{aligned} \quad (10)$$

where the correspondence $p \leftrightarrow t_1$ and $s \leftrightarrow \Delta t = t_2 - t_1$ applies for the Laplace transform; note that $\mathcal{L}[f(t_1 + \Delta t)](p, s) = \int_0^\infty dt_1 \int_0^\infty d\Delta t e^{-pt_1} e^{-s\Delta t} f(t_1 + \Delta t)$ can be rewritten as $\frac{\mathcal{L}[f(t_1)](p) - \mathcal{L}[f(\Delta t)](s)}{s - p}$, see for instance Ref. [35].

This is a very general result for the two-point density function, where the evolution for $\Delta t > 0$ depends on the pre-history of the system until time t_1 . It is therefore capable of describing processes with aging, in particular with run times, which follow a power-law distribution [32–34]. Formally, we have thus solved our random walk model analytically for any distribution $f(\tau)$ of run times. To calculate the correlation function $C_{rw}(t_1, t_2)$, one has to find the inverse Laplace transform of Eq. (10) with respect to p and s , and this sometimes presents a technical difficulty. To apply our result

to relevant biological examples, we will focus on two special cases, namely run times which follow an exponential or power-law distribution.

Exponential distribution of run times

We first consider an exponential run time distribution,

$$f(\tau) = \frac{1}{\tau_{\text{run}}} \exp\left(-\frac{\tau}{\tau_{\text{run}}}\right), \quad (11)$$

where $\tau_{\text{run}} = \int_0^\infty d\tau f(\tau)\tau$ is the mean run time. Since the exponential PDF is the memoryless distribution, Eq. (10) simplifies considerably. Performing two inverse Laplace transforms and using Eqs. (4, 8), we obtain a well-known result for the velocity autocorrelation function [36],

$$C_{\text{rw}}(t_1, t_2) = v^2 \exp\left(-\frac{|t_2 - t_1|}{\tilde{\tau}}\right), \quad \tilde{\tau} = \frac{\tau_{\text{run}}}{1 - \cos \varphi_0}, \quad (12)$$

which decays exponentially on the time scale $\tilde{\tau}$. It is plotted for run-and-tumble motion for *E. coli* ($\alpha = \langle \cos \varphi \rangle = 0.33$) and run-reverse ($\alpha = \langle \cos \varphi \rangle = -1$) in Fig. 3. With the help of Eq. (2), we find the MSD for the random walk pattern (without rotational diffusion),

$$\langle [\mathbf{r}(t) - \mathbf{r}(0)]^2 \rangle_{\text{rw}} = 2v^2 \tilde{\tau}^2 \left(\frac{t}{\tilde{\tau}} - 1 + e^{-t/\tilde{\tau}} \right), \quad (13)$$

whose analytical form also arises from the Ornstein-Uhlenbeck process of a Brownian particle [37]. Note that, up to this point, our results were derived for the model in $d=2$. In Sec. III of Text S1, we show that Eq. (13) is also valid for $d=3$. Therefore, below we use $d=3$ to compute the diffusion constant and compare with known results. For small times $t \ll \tilde{\tau}$, the MSD from Eq. (13) describes ballistic motion; for large times $t \gg \tilde{\tau}$, the MSD scales linearly in time, $\langle [\mathbf{r}(t) - \mathbf{r}(0)]^2 \rangle_{\text{rw}} \sim 6Dt$ (see Fig. 4), with diffusion coefficient [13,36]

$$D = \frac{v^2 \tau_{\text{run}}}{3(1 - \cos \varphi_0)}. \quad (14)$$

Note that the regime of reversals, where cells backtrack along their previous path, has a minimal diffusion constant, which is two times smaller than in the case of completely random reorientations with $\cos \varphi_0 = 0$. The limiting case of $\varphi_0 = 0^\circ$ generates ballistic motion, such that D diverges. However, this divergence can be regularized by rotational diffusion during the run events. As a consequence of Eq. (7), the full velocity autocorrelation function then becomes

$$C(t_1, t_2) = v^2 \exp\left(-\frac{|t_2 - t_1|}{\tau_{\text{eff}}}\right), \quad (15)$$

which gives rise to the characteristic time scale $\tau_{\text{eff}} = \frac{\tilde{\tau} \tau_{\text{rot}}}{\tilde{\tau} + \tau_{\text{rot}}}$, or

$$\frac{1}{\tau_{\text{eff}}} = \frac{1}{\tilde{\tau}} + \frac{1}{\tau_{\text{rot}}}. \quad (16)$$

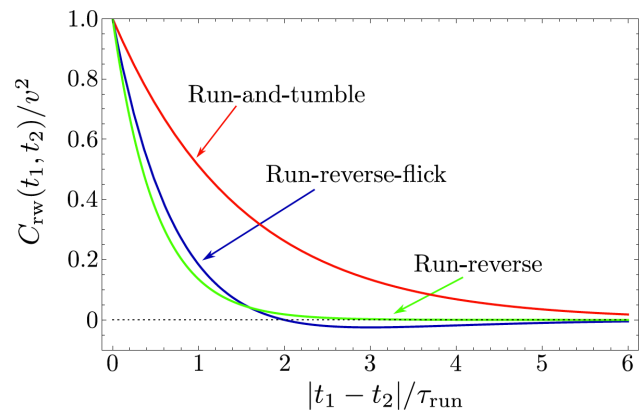


Figure 3. Velocity correlation function. The normalized velocity correlation function $C_{\text{rw}}(t_1, t_2)/v^2$ is plotted as a function of dimensionless time $|t_1 - t_2|/\tau_{\text{run}}$. The curves are shown for run-and-tumble of *E. coli* with persistence parameter $\alpha = 0.33$ (red), run-reverse with $\alpha = -1$ (green), and run-reverse-flick with alternating $\alpha = -1$ and $\alpha = 0$ (blue). The analytical expressions are given in Eqs. (12) and (21), respectively.

doi:10.1371/journal.pone.0081936.g003

Power-law distribution of run times

In Refs. [21,22], it was pointed out that cells of *E. coli* can have power-law distributed run times,

$$f(\tau) = \frac{\gamma}{\tau_0(1 + \tau/\tau_0)^{1+\gamma}}, \quad (17)$$

with exponent $\gamma \approx 1.2$. The power-law distribution (17) leads to a finite mean run time $\langle \tau \rangle = \tau_0/(\gamma - 1)$ (for $\gamma > 1$), but the average of the squared run length diverges, leading to anomalous diffusion [35]. Also because of the power-law tail in the distribution of run times, memory effects play a significant role in the transport process. This means that the probability that a cell tumbles within a small time interval depends on its history. However, with the help of the general expression Eq. (10), which explicitly takes into account these memory effects, we can calculate $C_{\text{rw}}(t_1, t_2)$. The double inverse Laplace transform required to compute the correlation function in the real time domain presents a technical challenge, which can be resolved numerically. Analytically, it is

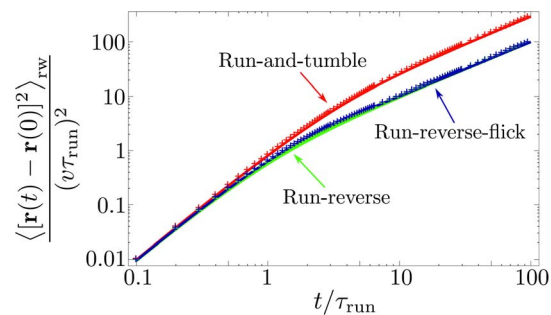


Figure 4. Mean squared displacement (MSD). The curves of the normalized MSD versus dimensionless time t/τ_{run} correspond to *E. coli*'s run-and-tumble with $\alpha = 0.33$ (red), run-reverse with $\alpha = -1$ (green), and run-reverse-flick with alternating $\alpha = -1$ and $\alpha = 0$ (blue). The analytical expressions are given in Eqs. (13) and (22), respectively. The crosses are obtained from numerical simulations and fully agree with the analytical results.

doi:10.1371/journal.pone.0081936.g004

possible to consider the asymptotic behavior of the correlation function for large t_1 and Δt (corresponding to the limit $p, s \rightarrow 0$ in Laplace space). An asymptotic analysis for $1 < \gamma < 2$ leads to

$$C_{rw}(t_1, t_2) \simeq v^2 \left[\left(1 + \frac{|t_2 - t_1|}{\tau_0} \right)^{1-\gamma} - \left(1 + \frac{\max(t_2, t_1)}{\tau_0} \right)^{1-\gamma} \right], \quad (18)$$

valid for large t_1, t_2 , and $|t_2 - t_1|$. One of the remarkable results here is that in the asymptotic regime the correlation function and therefore the MSD do not depend on the turning angle distribution: Long persistent runs dominate over geometric effects. From Eq. (18), it follows that the MSD displays superdiffusive behavior for large times, when the MSD grows faster than linearly in time: $\langle [\mathbf{r}(t) - \mathbf{r}(0)]^2 \rangle_{rw} \propto t^{3-\gamma}$. In fact, the trajectories of bacteria in this regime represent a two-dimensional realization of a Lévy walk [35,38]. If we now consider rotational diffusion during the runs it makes the dispersal normal again and for large times the MSD scales linearly in time.

Random walk with alternating turning angles: Run-reverse-flick

We now discuss the motility pattern, which is represented by the alternation of a forward run, reversal event, backward run, and flick event. The angular jump distribution from Eq. (3) is thus different for reversal and flick angles,

$$g_{r,f}(\varphi) = \frac{1}{2} \left[\delta(\varphi - \varphi_{r,f}) + \delta(\varphi + \varphi_{r,f}) \right], \quad (19)$$

with $\varphi_r = 180^\circ$ and $\varphi_f = 90^\circ$. We also allow for two different distributions for run times after reversals $f_r(\tau)$ and after flicks $f_f(\tau)$.

To determine the joint probability density P , we formulate and solve the full set of equations of the underlying CTRW for the direction $\varphi(t)$. In Sec. I of Text S1, we sketch the derivation and present our analytical result for the two-point PDF P . It is exact and holds for arbitrary run time and turning angle distributions in its most general form. In the following, we restrict our study to the experimentally relevant case of exponential distributions, as given in Eq. (11), but we allow for two different mean values τ_r and τ_f , corresponding to run times after reversal and flick events, respectively. Our approach yields an exact analytical result for the velocity autocorrelation function,

$$C_{rw}(t_1, t_2) = \frac{\tau_f(\tau_f - 2\tau_r) \exp\left(-\frac{|t_2 - t_1|}{\tau_f}\right) - \tau_r(\tau_r - 2\tau_f) \exp\left(-\frac{|t_2 - t_1|}{\tau_r}\right)}{v^2 (\tau_f - \tau_r)(\tau_f + \tau_r)}. \quad (20)$$

For *V. alginolyticus*, the mean run times are similar with $\tau_r \sim \tau_f \sim 0.3$ s. For a single run time $\tau_{run} = \tau_r = \tau_f$, Eq. (20) then reduces to

$$C_{rw}(t_1, t_2) = v^2 \left(1 - \frac{|t_2 - t_1|}{2\tau_{run}} \right) \exp\left(-\frac{|t_2 - t_1|}{\tau_{run}}\right). \quad (21)$$

A peculiar feature of this correlation function is that it becomes negative for $|t_2 - t_1| > 2\tau_{run}$, see also Fig. 3. Note that for the run-reverse pattern without flicks, the correlations are always positive, see Eq. (12). Next, we use Eq. (21) to obtain the expression for the MSD,

$$\langle [\mathbf{r}(t) - \mathbf{r}(0)]^2 \rangle_{rw} = v^2 \tau_{run} t \left(1 - e^{-t/\tau_{run}} \right). \quad (22)$$

The functional form of this MSD is different from the corresponding expression for the random walk with a single turning angle [Eq. (13)]. However, it is striking that the resulting diffusion coefficient $D = v^2 \tau_{run} / 6$ is identical for run-reverse and run-reverse-flick motion, see Fig. 4. This degeneracy vanishes if rotational diffusion during the runs is taken into account; the diffusion coefficient then reads (for $d = 3$)

$$D = \frac{v^2}{6} \frac{1/\tau_{run} + 2/\tau_{rot}}{(1/\tau_{run} + 1/\tau_{rot})^2}, \quad (23)$$

and, in general, $D_{run-rev-flick} \geq D_{run-rev}$. It is instructive to present the result for the diffusion coefficient with $\tau_r \neq \tau_f$ (for details, see Sec. I of Text S1):

$$D = \frac{v^2}{3} \frac{\tau_r^2 - \tau_r \tau_f (1 - 2D_r \tau_r) + \tau_f^2 (1 + 2D_r \tau_r)}{(\tau_r + \tau_f)(1 + 2D_r \tau_r)(1 + 2D_r \tau_f)}. \quad (24)$$

The exact answers (23) and (24) differ from previous simple estimates [16,19,39]. For example, an intuitive attempt to use an average value of $\cos(180^\circ)$ and $\cos(90^\circ)$ and substitute it into Eq. (14) [19] yields an incorrect result. We also see that the diffusion constant does not vanish when $\tau_r \sim \tau_f$, cf. [16].

Comparison of the diffusion coefficient for *E. coli* and *V. alginolyticus*. As typical parameters, we set $v = 19 \mu\text{m s}^{-1}$ and $\tau_{run} = 1$ s for *E. coli*, and $v = 45 \mu\text{m s}^{-1}$ and $\tau_{run} = 0.3$ s for *V. alginolyticus* [13,16,24,40]. A realistic rotational diffusion constant, which is applicable to both types of bacteria, is $D_r = 0.2 \text{ rad}^2 \text{ s}^{-1}$ [16,41]. With these numbers, the diffusion coefficients (in $d = 3$) read

$$E. coli \quad D = 112 \mu\text{m}^2 \text{ s}^{-1},$$

$$V. alginolyticus \quad D = 101 \mu\text{m}^2 \text{ s}^{-1}.$$

Note that the diffusion coefficient is sensitive to the rotational diffusion constant D_r if the mean run time is comparable to the time scale of rotational diffusion $\tau_{rot} = 1/(2D_r) = 2.5$ s, as is the case for *E. coli*. For example, the diffusion coefficient of *E. coli* becomes $D = 180 \mu\text{m}^2 \text{ s}^{-1}$, if we neglect rotational diffusion and set $D_r = 0$.

This demonstrates how the rigorous theoretical model can quantitatively describe the dispersal of bacteria in a homogeneous environment. We next investigate the process of chemotaxis.

Chemotaxis

If a bacterium, such as *E. coli*, is exposed to a gradient of chemoattractant, for example amino acids or sugars, with concentration c , it changes its unbiased run-and-tumble strategy in order to move along the gradient [13]. To do so, the genetic chemotactic pathway of *E. coli* extends the run times if the cell swims in the direction of increasing concentration ∇c [14]. The bacterial response to a short pulse of chemoattractant is measured by the fraction of time that a flagellum tethered to a surface rotates CCW [42]; the response reveals a biphasic behavior. After the stimulation with the chemical pulse, the fraction quickly reaches a maximum and remains above the baseline for ~ 1 s, then it falls

below and finally approaches the baseline after ~ 4 s [15]. The shape of this curve for the fraction of CCW rotation motivated the introduction of a response function $R(t)$. In Ref. [43], the response function was used to linearly connect the tumbling rate $\lambda(t)$ of a bacterium to the concentration of chemicals it experienced along its path,

$$\lambda(t) = \lambda \left(1 - \int_{-\infty}^t dt' c(t') R(t-t') \right), \quad (25)$$

where $\lambda = 1/\tau_{\text{run}}$ is the cell's tumbling rate in a homogeneous environment. In fact, $\lambda(t)$ hardly increases when a cell moves against the gradient [14,15]; however, we use the full expression from Eq. (25) and note that our calculations could also be modified to account for this detail. In this paper, we employ the following analytical expression for the response function, which was frequently used in previous work [41,44,45]:

$$R(t) = W \lambda e^{-\lambda t} \left[1 - \frac{\lambda t}{2} - \left(\frac{\lambda t}{2} \right)^2 \right], \quad t \geq 0. \quad (26)$$

Here, we introduce a single normalization constant W with the dimension of volume. One of the interesting features of $R(t)$ is that it satisfies the adaptive response property $\int_0^\infty dt R(t) = 0$.

In Ref. [46], de Gennes used Eq. (25) and a perturbation theory approach to calculate the chemotactic drift velocity of bacteria, $v_d = \lim_{t \rightarrow \infty} \langle \mathbf{r}(t) - \mathbf{r}(0) \rangle / t$, in the presence of a small gradient $|\nabla c|$. This result was generalized by Locsei for *E. coli* by including the directional persistence between tumbling events and rotational diffusion during runs [45]. Note that the result is fully consistent with the different approach by Celani and Vergassola from Ref. [41]: The authors also assume the tumbling rate from Eq. (25), but they introduce additional Markovian internal variables and arrive at a Fokker-Planck description. The hydrodynamic limit provides expressions for the chemotactic sensitivity $\chi = v_d / |\nabla c|$ and bacterial diffusivity D . The directionality parameter $\omega \approx 1$ from [41] corresponds to our persistence parameter $\alpha = 1/3$ —the value of *E. coli*—, and using the adaptive response property, both the diffusion constant and chemotactic sensitivity from [41] agree with [13,36,45].

Using the response function from Eq. (26), the drift speed $v_d = |v_d|$ is given by [45]

$$v_d = |\nabla c| W v^2 \frac{\lambda^2 [\lambda(5-2\alpha) + 4D_r](1-\alpha)}{6[2D_r + \lambda(1-\alpha)][2D_r + \lambda(2-\alpha)]^3}. \quad (27)$$

This is plotted as a function of $\alpha = \langle \cos \phi \rangle$ in Fig. 5 (red curve). We are primarily interested in the effect of the motility pattern on the chemotactic drift speed v_d . Therefore, we use the chemotactic response function of *E. coli* for our modeling; to the best of our knowledge, it is also the only experimentally measured one. However, we recall that the chemotactic response of bacteria, such as *E. coli*, *B. subtilis*, or *R. sphaeroides*, has been recently modeled on a biochemical level [47,48].

Chemotactic drift speed for run-tumble-flick motion

We want to compare the chemotactic drift speed of run-and-tumble with persistence parameter $\alpha = \langle \cos \phi \rangle$ to a random walk, where one turn happens with the same α , but every second angular change stems from a flick, which destroys any directional

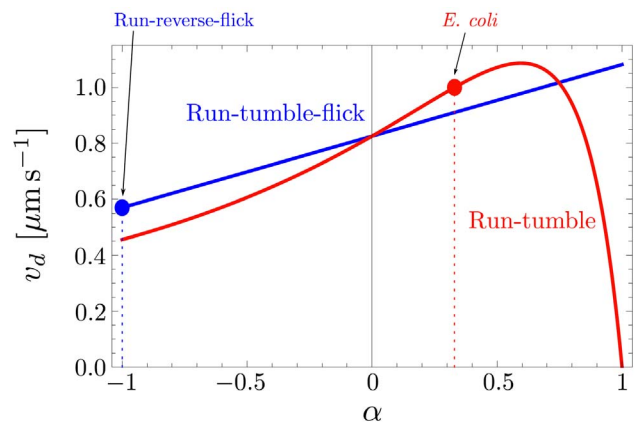


Figure 5. Comparison of the chemotactic drift speed v_d versus persistence parameter α between run-tumble-flick [Eq. (28)] and run-tumble [Eq. (27)]. All parameters are adjusted to *E. coli* in the gradient $|\nabla c| = 1 \mu\text{m}^{-4}$ with $\lambda = 1 \text{ s}^{-1}$, $v = 19 \mu\text{m s}^{-1}$, $D_r = 0.2 \text{ s}^{-1}$, and $W = 0.0458 \mu\text{m}^3$.

doi:10.1371/journal.pone.0081936.g005

persistence. We denote the second pattern as “run-tumble-flick”; setting $\alpha = -1$ yields the run-reverse-flick strategy.

Now it is important to consider the motion of cells in three dimensions. We assume a small chemical gradient $|\nabla c|$ in the z direction, and the concentration $c(t)$, which is experienced by the bacterium at position $z(t)$, becomes $c(t) = |\nabla c| z(t)$. In the simplest case, the times for runs after tumbles and flicks are equally distributed with mean $\tau_{\text{run}} = \lambda^{-1}$. We then take the approach from Eq. (25) and perform a calculation of v_d in the spirit of Refs. [45,46]: To first order in $|\nabla c|$, we determine the mean displacement during a forward and subsequent backward run, $\langle z \rangle$, which yields the chemotactic drift speed $v_d = \langle z \rangle / (2\tau_{\text{run}})$. We arrive at the following result (see Ref. [49] and Sec. IV of Text S1 for details):

$$v_d = |\nabla c| W v^2 \lambda^2 \frac{16D_r^3(2-\alpha) + 4\lambda D_r^2(22-5\alpha) + 2\lambda^2 D_r(38+5\alpha) + \lambda^3(20+11\alpha)}{192(\lambda + D_r)^4(\lambda + 2D_r)^2}. \quad (28)$$

The chemotactic drift speed v_d is always positive and a linear function of α (see the blue curve in Fig. 5). The red curve of Fig. 5 shows v_d for the same parameters but without flicks. For negative persistence parameter α , the additional flick event helps the random walker to approach the gradient better, and v_d is larger with a flick for $\alpha < 0$. For $\alpha = 0$, both random walk processes are equal as they have no persistence, and the curves intersect. For increasing $\alpha > 0$, v_d is smaller in the presence of the randomizing flick event. Finally, there is a pronounced difference at $\alpha = 1$, where $v_d = 0$ for the run-and-tumble strategy, while v_d becomes maximal for run-tumble-flick motion. This is easy to understand since the $\alpha = 1$ in the run-and-tumble model entails no turning events for the cell and the cell is not able to move actively in the direction of the gradient. An additional flick clearly allows the cell to reorient.

Note that a similar calculation for the run-reverse-flick pattern is also found in Ref. [39], where the chemotactic drift is determined only for the delta-response $R(t) \propto \delta(t-T)$ and without rotational diffusion. Our result in Eq. (28) is based on the response function of *E. coli* and explicitly shows the influence of rotational diffusion on the chemotactic drift speed.

Comparison of the chemotactic drift speed for *E. coli* and *V. alginolyticus*. In recent experimental work [24], the chemotactic drift velocity of *E. coli* in a constant gradient of the amino acid serine was measured. It is important to note that the perturbative nature of the analysis we used to calculate the drift velocity assumes a very small gradient. An obvious limitation on the gradient arises from Eq. (25), where the rate $\lambda(t)$ cannot become negative. Therefore, we use the value of the drift speed for the smallest measured gradient (see Sec. II of Text S1) and formula (27) to calculate the only remaining unknown parameter $W=0.0458 \mu\text{m}^3$. As before, we use $v=19 \mu\text{m s}^{-1}$, $\lambda=1 \text{ s}^{-1}$ for *E. coli*, and $v=45 \mu\text{m s}^{-1}$, $\lambda=3.3 \text{ s}^{-1}$ for *V. alginolyticus*. Rotational diffusion is set to $D_r=0.2 \text{ rad}^2 \text{ s}^{-1}$, and the value of the gradient is $|\nabla c|=1 \mu\text{m}^{-4}$. Finally, we stress that we choose the same shape and prefactor W of the response function for both bacteria.

For *E. coli*, the chemotactic drift speed then becomes $v_d=1 \mu\text{m s}^{-1}$. For *V. alginolyticus*, we obtain the larger value $v_d=1.23 \mu\text{m s}^{-1}$. For smaller values with $D_r \sim 0.14 \text{ rad}^2 \text{ s}^{-1}$, the chemotactic drift speed of *V. alginolyticus* becomes smaller than that of *E. coli*; as in the above case, for sufficiently large D_r , the winner of the chemotaxis race is the run-reverse-flick swimmer *V. alginolyticus*, see Fig. 6. However, as the swimming speed of *V. alginolyticus* $v=45 \mu\text{m s}^{-1}$ is more than twice that of *E. coli* $v=19 \mu\text{m s}^{-1}$, we also compare the chemotactic index, defined by v_d/v . For $D_r=0.2 \text{ rad}^2 \text{ s}^{-1}$ or smaller values, v_d/v for *E. coli* (5.3%) is almost twice as large as for *V. alginolyticus* (2.7%). In this sense, the relative chemotaxis race trophy goes to *E. coli*. Ref. [19] reports the experimental observation that “*V. alginolyticus* has a threefold larger chemotactic velocity than *E. coli*.” Our analytical results clearly show that the motility pattern alone cannot explain the threefold difference in the chemotactic behavior observed experimentally. In fact, the only unknown in our model is the response function of *V. alginolyticus* bacteria, which for the sake of comparison we set to be the same as of *E. coli*. It is therefore natural to conclude that a different response function of *V. alginolyticus* is the key to interpret the experimental data of Ref. [16].

Discussion

We have demonstrated how the careful analysis of bacterial motility patterns could quantitatively describe the dispersal of cells in homogeneous environments and the chemotactic drift velocity

in small gradients of signaling chemicals. When the characteristic length scale on which the chemical concentration changes is much larger than the average run length of the cell, it is possible to use a continuous description for the density of cells $\rho(\mathbf{r},t)$. Its dynamics can be described by an advection-diffusion equation, as part of the Keller-Segel model for chemotactic aggregation [50], where the drift term represents the effect of chemotaxis and biases the otherwise uniform spreading of cells,

$$\partial_t \rho = D \nabla^2 \rho - \nabla(\rho \chi \nabla c). \quad (29)$$

Here, $c(\mathbf{r},t)$ denotes the chemical field and $\chi = v_d/|\nabla c|$ is defined as the chemotactic sensitivity and assumed to be constant. We can consider an oversimplified setting of an infinite one-dimensional domain with an imposed gradient of the chemical and find a stationary solution for this problem. One can show that the density of cells follows the profile of the chemical and has the following shape:

$$\rho(r) \propto \exp\left(\frac{\chi}{D} c(r)\right). \quad (30)$$

This stationary profile depends on the ratio of the chemotactic drift coefficient χ and diffusion constant D . If we estimate this ratio for *E. coli* and *V. alginolyticus*, again assuming the same response function, they appear to be remarkably close to each other: $\chi/D=0.009 \mu\text{m}^3$ (*E. coli*), $\chi/D=0.012 \mu\text{m}^3$ (*V. alginolyticus*). This result cannot be directly compared to the available experimental data [16], where gradients are very steep and the characteristic width of the cloud of cells around the source of the chemoattractant becomes comparable to the average length of the cell run. Nevertheless, the significantly different extensions of the cell clumps forming around the source hint to a difference in the response function between the two bacterial species (and not the motility pattern) as the reason for the observed behavior.

It appears that many cells, which are able to perform chemotaxis, have the motility patterns discussed in this paper. In particular, our analytical approach is not limited to the bacterial world, but can also be applied to swimming algae [51], cells moving during the early stages of embryo development [52], or artificial nano swimmers [53] — all of them demonstrating a very similar motility pattern. There are some examples, like swimming *P. putida* bacteria, which in addition to a reversal have also two different speeds for backward and forward motion [54]. With

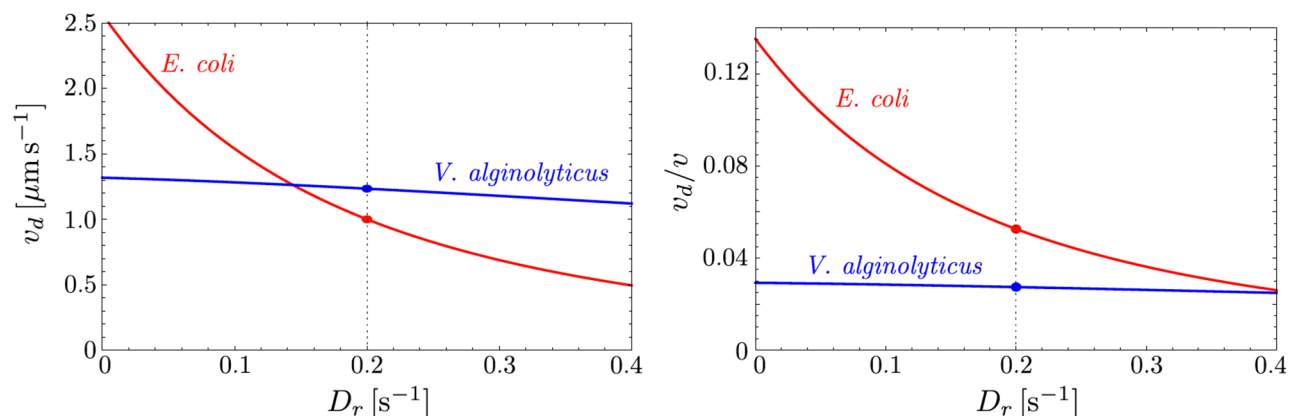


Figure 6. Chemotactic drift speed as a function of D_r for *E. coli* and *V. alginolyticus*. The plot on the left shows v_d ; on the right, the chemotactic drift is normalized by the swimming speed as v_d/v and coincides with the chemotactic index. doi:10.1371/journal.pone.0081936.g006

some minor modifications such a scenario can easily be incorporated into the framework developed here. The fact that the motility pattern of cells is now accounted for rigorously, makes it possible to apply the model to the existing data on drift velocities or agglomeration experiments [8,16]. This way, it is feasible to access the characteristics of cells, like the response function, which would require much more sophisticated experiments to be measured directly. The response functions of various bacteria might have different functional forms or different strengths and depend on the chemical nature of the signal. We believe that our theoretical framework, complemented by numerical simulations, may serve as an excellent tool to test various hypotheses regarding the response of bacteria and check their consistency with experimental data for various motility patterns of bacteria observed in nature and laboratory.

References

- Whitman WB, Coleman DC, Wiebe WJ (1998) Prokaryotes: The unseen majority. *Proc Natl Acad Sci USA* 95: 6578–6583.
- Kearns DB (2010) A field guide to bacterial swarming motility. *Nat Rev Microbiol* 8: 634–644.
- Hall-Stoodley L, Costerton JW, Stoodley P (2002) Bacterial biofilms: from the natural environment to infectious diseases. *Nat Rev Microbiol* 2: 95–108.
- O'Toole G, Kaplan HB, Kolter R (2000) Biofilm formation as microbial development. *Annu Rev Microbiol* 54: 49–79.
- Eisenbach M (2004) Chemotaxis. London: Imperial College Press, 1 edition.
- Hazelbauer GL (2012) Bacterial chemotaxis: The early years of molecular studies. *Annu Rev Microbiol* 66: 285–303.
- Turner L, Ryu WS, Berg HC (2000) Real-time imaging of fluorescent agellar filaments. *J Bacteriol* 182: 2793–2801.
- Barbara GM, Mitchell JG (2003) Bacterial tracking of motile algae. *FEMS Microbiol Ecol* 44: 79–87.
- Whitworth DE, editor (2008) Myxobacteria: Multicellularity and Differentiation. Washington: ASM Press.
- Wu Y, Kaiser AD, Jiang Y, Alber MS (2009) Periodic reversal of direction allows myxobacteria to swarm. *Proc Natl Acad Sci USA* 106: 1222–1227.
- Rashid MH, Kornberg A (2000) Inorganic polyphosphate is needed for swimming, swarming, and twitching motilities of *Pseudomonas aeruginosa*. *Proc Natl Acad Sci USA* 97: 4885–4890.
- Caiazza NC, Merritt JH, Brothers KM, O'Toole GA (2007) Inverse regulation of biofilm formation and swarming motility by *Pseudomonas aeruginosa* pa14. *J Bacteriol* 189: 3603–3612.
- Berg HC (1993) *Random Walks in Biology*. Princeton: Princeton University Press.
- Berg HC, Brown DA (1972) Chemotaxis in *Escherichia coli* analysed by three-dimensional tracking. *Nature* 239: 500–504.
- Berg HC (2004) *E. coli* in motion. New York: Springer.
- Xie L, Altindal T, Chattopadhyay S, Wu XL (2011) Bacterial flagellum as a propeller and as a rudder for efficient chemotaxis. *Proc Natl Acad Sci USA* 108: 2246–2251.
- Son K, Guasto JS, Stocker R (2013) Bacteria can exploit a flagellar buckling instability to change direction. *Nat Phys* 9: 494–498.
- Berg HC (2013) Cell motility: Turning failure into function. *Nat Phys* 9: 460–461.
- Stocker R (2011) Reverse and flick: Hybrid locomotion in bacteria. *Proc Natl Acad Sci USA* 108: 2635–2636.
- Kafri Y, da Silveira RA (2008) Steady-state chemotaxis in *Escherichia coli*. *Phys Rev Lett* 100: 238101.
- Korobkova E, Emonet T, Vilar JMG, Shimizu TS, Cluzel P (2004) From molecular noise to behavioural variability in a single bacterium. *Nature* 428: 574–578.
- Tu Y, Grinstein G (2005) How white noise generates power-law switching in bacterial flagellar motors. *Phys Rev Lett* 94: 208101.
- Masson JB, Voisinne G, Wong-Ng J, Celani A, Vergassola M (2012) Noninvasive inference of the molecular chemotactic response using bacterial trajectories. *Proc Natl Acad Sci USA* 109: 1802–1807.
- Vuppula RR, Tirumkudulu MS, Venkatesh KV (2010) Chemotaxis of *Escherichia coli* to l-serine. *Phys Biol* 7: 026007.
- Johansen JE, Pinhassi J, Blackburn N, Zweifel UL, Hagström A (2002) Variability in motility characteristics among marine bacteria. *Aquat Microb Ecol* 28: 229–237.
- Magariyama Y, Ichiba M, Nakata K, Baba K, Ohtani T, et al. (2005) Difference in bacterial motion between forward and backward swimming caused by the wall effect. *Biophys J* 88: 3648–3658.
- Mitchell JG, Pearson L, Dillon S, Kantalis K (1995) Natural assemblages of marine bacteria exhibiting high-speed motility and large accelerations. *Appl Environ Microbiol* 61: 4436–40.

Supporting Information

Text S1 How the motility pattern of bacteria affects their dispersal and chemotaxis.

(PDF)

Acknowledgments

We thank Frank Jülicher, Pablo A. Iglesias, and Louise Jawerth for critically reading the manuscript and discussions. JT and VZ are grateful to David A. Weitz for fruitful discussions and supporting their research during their stay with his group at Harvard University.

Author Contributions

Wrote the paper: JT HS VZ. Designed the research: JT HS VZ. Performed the research: JT VZ.

- Skerker JM, Berg HC (2001) Direct observation of extension and retraction of type IV pili. *Proc Natl Acad Sci USA* 98: 6901–6904.
- Romanczuk P, Bär M, Ebeling W, Lindner B, Schimansky-Geier L (2012) Active brownian particles. *Eur Phys J Spec Top* 202: 1–162.
- Taktikos J, Zaboruaev V, Stark H (2011) Modeling a self-propelled autochemotactic walker. *Phys Rev E* 84: 041924.
- Doi M, Edwards SF (2001) *The theory of polymer dynamics*. Oxford: Clarendon Press.
- Zaboruaev V (2008) Microscopic approach to random walks. *J Stat Phys* 133: 159–167.
- Baule A, Friedrich R (2007) A fractional diffusion equation for two-point probability distributions of a continuous-time random walk. *Europhys Lett* 77: 10002.
- Barkai E, Sokolov IM (2007) Multi-point distribution function for the continuous time random walk. *J Stat Mech* 2007: P08001.
- Klafter J, Sokolov IM (2011) *First Steps in Random Walks - From Tools to Applications*. Oxford: Oxford University Press.
- Lovely PS, Dahlquist FW (1975) Statistical measures of bacterial motility and chemotaxis. *J Theor Biol* 50: 477–496.
- Risken H (1996) *The Fokker-Planck Equation*. New York: Springer, 2 edition.
- Thiel F, Schimansky-Geier L, Sokolov IM (2012) Anomalous diffusion in run-and-tumble motion. *Phys Rev E* 86: 021117.
- Altindal T, Xie L, Wu XL (2011) Implications of three-step swimming patterns in bacterial chemotaxis. *Biophys J* 100: 32–41.
- Vuppula RR, Tirumkudulu MS, Venkatesh KV (2010) Mathematical modeling and experimental validation of chemotaxis under controlled gradients of methyl-aspartate in *Escherichia coli*. *Mol BioSyst* 6: 1082–1092.
- Celani A, Vergassola M (2010) Bacterial strategies for chemotaxis response. *Proc Natl Acad Sci USA* 107: 1391–1396.
- Segall JE, Block SM, Berg HC (1986) Temporal comparisons in bacterial chemotaxis. *Proc Natl Acad Sci USA* 83: 8987–8991.
- Schnitzer MJ (1993) Theory of continuum random walks and application to chemotaxis. *Phys Rev E* 48: 2553–2568.
- Clark DA, Grant LC (2005) The bacterial chemotactic response reverts a compromise between transient and steady-state behavior. *Proc Natl Acad Sci USA* 102: 9150–9155.
- Locsei J (2007) Persistence of direction increases the drift velocity of run and tumble chemotaxis. *J Math Biol* 55: 41–60.
- de Gennes PG (2004) Chemotaxis: the role of internal delays. *Eur Biophys J* 33: 691–693.
- Rao CV, Kirby JR, Arkin AP (2004) Design and diversity in bacterial chemotaxis: A comparative study in *Escherichia coli* and *Bacillus subtilis*. *PLoS Biol* 2: e49.
- Hamadeh A, Roberts MAJ, August E, McSharry PE, Maini PK, et al. (2011) Feedback control architecture and the bacterial chemotaxis network. *PLoS Comput Biol* 7: e1001130.
- Taktikos J (2013) Modeling the random walk and chemotaxis of bacteria: Aspects of biofilm formation. Ph.D. thesis, Technische Universität Berlin.
- Horstmann D (2003) From 1970 until present: the Keller-Segel model in chemotaxis and its consequences. *I Jahresberichte DMV* 105: 103–165.
- Bennett RR, Golestanian R (2013) Emergent run-and-tumble behavior in a simple model of *Chlamydomonas* with intrinsic noise. *Phys Rev Lett* 110: 148102.
- Blaser H, Reichman-Fried M, Castanon I, Dumstrei K, Marlow FL, et al. (2006) Migration of zebrafish primordial germ cells: A role for myosin contraction and cytoplasmic flow. *Dev Cell* 11: 613–627.
- Ebbens SJ, Buxton GA, Alexeev A, Sadeghi A, Howse JR (2012) Synthetic running and tumbling: an autonomous navigation strategy for catalytic nanoswimmers. *Soft Matter* 8: 3077–3082.
- Theves M, Taktikos J, Zaboruaev V, Stark H, Beta C (2013) A bacterial swimmer with two alternating speeds of propagation. *Biophys J* 105: 1915–1924.